

**Brightening of dark excitons in WS<sub>2</sub> via tensile strain-induced excitonic valley convergence**

Tamaghna Chowdhury <sup>1,2,\*</sup> Sagnik Chatterjee <sup>2</sup> Dibyasankar Das <sup>3</sup> Ivan Timokhin <sup>1,4</sup> Pablo Díaz Núñez <sup>1,4</sup>  
Gokul M. A. <sup>2</sup> Suman Chatterjee <sup>5</sup> Kausik Majumdar <sup>5</sup> Prasenjit Ghosh <sup>2,6</sup>  
Artem Mishchenko <sup>1,4,†</sup> and Atikur Rahman <sup>2,‡</sup>

<sup>1</sup>Department of Physics and Astronomy, *University of Manchester, Manchester M13 9PL, United Kingdom*

<sup>2</sup>Department of Physics, *Indian Institute of Science Education and Research, Pune 411008, India*

<sup>3</sup>Department of Condensed Matter Physics and Material Science, *Tata Institute of Fundamental Research, Mumbai 400005, India*

<sup>4</sup>National Graphene Institute, *University of Manchester, Manchester M13 9PL, United Kingdom*

<sup>5</sup>Department of Electrical Communication Engineering, *Indian Institute of Science, Bangalore 560012, India*

<sup>6</sup>Department of Chemistry, *Indian Institute of Science Education and Research, Pune 411008, India*



(Received 8 March 2024; revised 20 June 2024; accepted 25 July 2024; published 12 August 2024)

Transition-metal dichalcogenides (TMDs) host tightly bound electron-hole pairs—excitons—which can be either optically bright or dark based on spin and momentum selection rules. In tungsten-based TMDs, a momentum-forbidden dark exciton is the energy ground state, and therefore, it strongly affects the emission properties. In this work, we brighten the momentum-forbidden dark exciton by placing monolayer tungsten disulfide on top of nanotextured substrates, which imparts tensile strain, modifying its electronic band structure. This enables phonon-assisted exciton scattering between momentum valleys, thereby brightening momentum-forbidden dark excitons. In addition to offering a tuning knob for light-matter interactions in two-dimensional materials, our results pave the way for designing ultrasensitive strain-sensing devices based on TMDs.

DOI: [10.1103/PhysRevB.110.L081405](https://doi.org/10.1103/PhysRevB.110.L081405)

Transition-metal dichalcogenides (TMDs; e.g.,  $MX_2$ ,  $M = \text{Mo, W}$ ,  $X = \text{S, Se}$ ) are known for their novel optical properties [1]. They host excitons, charge-neutral electron-hole pairs bound by Coulomb interactions [2–7]. The large spin-orbit coupling in tungsten disulfide (WS<sub>2</sub>), due to the heavy mass of the tungsten atom, splits the valance band maximum (VBM) at the  $K$  point and conduction band minimum (CBM) at the  $K$  and  $\Lambda$  points in two subbands with opposite spin orientations. This results in the formation of “bright” intravalley  $KK$  excitons with the hole at the upper subband of the  $K$  VBM and an electron at the upper subband of the  $K$  CBM [CBM + 1; Fig. 1(a)]. There is also the possibility for the formation of indirect intervalley  $K\Lambda$  excitons with the hole in the upper subband of the  $K$  VBM and the electron in the lower subband of the  $\Lambda$  CBM as well [Fig. 1(a)] [8,9]. But because of the large momentum mismatch, they require the assistance of phonons to recombine radiatively [10]. The  $K\Lambda$  exciton is therefore called a momentum-forbidden dark exciton [11]. In the case of W-based monolayer (ML) TMDs, the  $K\Lambda$  exciton is the excitonic ground state; it has a higher binding energy and longer lifetime than the  $KK$  bright excitons [11–13]. Therefore,  $K\Lambda$  exciton plays an important role in the exciton dynamics of the system. Thus, controlling them is essential for designing novel optical devices. The dark exciton can be brightened by exciton-phonon coupling if the energy of the available phonon mode matches the dark-bright exciton

energy splitting, which can be effectively tuned by applying strain to ML WS<sub>2</sub> [12,14,15]. Therefore, strain acts as a tuning knob for the emission of dark excitons [12,16,17].

Recent theoretical and experimental works predicted that the dark  $K\Lambda$  exciton in WS<sub>2</sub> can be brightened only by applying compressive strain [12,13]. Conversely, two recent studies [18,19] reported the existence of dark  $K\Lambda$  excitons in WSe<sub>2</sub> under tensile strain. However, in those works either the mechanism behind the brightening was not addressed [12,18], or it remained elusive due to the various approximations used in its description, such as not taking the binding energy of the  $K\Lambda$  exciton into account [13,19]. It is highly unlikely that two W-based materials will behave differently in terms of strain-mediated brightening of  $K\Lambda$  dark excitons, i.e., requiring compressive strain for WS<sub>2</sub> and tensile strain for WSe<sub>2</sub>, despite having similar excitonic band structures with  $K\Lambda$  dark excitons as the excitonic ground state in W-based TMDs (unlike in Mo-based TMDs) [8]. In this work, we experimentally show that the  $K\Lambda$  dark exciton can be brightened in ML WS<sub>2</sub> by the application of tensile strain. We perform temperature-dependent photoluminescence (PL) and Raman measurements on the strained and unstrained ML WS<sub>2</sub> samples. Supported by *ab initio* density functional theory (DFT) based calculations, we put forward a mechanism for the brightening of  $K\Lambda$  dark excitons through exciton-phonon coupling upon the application of tensile strain. Here, we apply tensile strain to ML WS<sub>2</sub> by placing ML WS<sub>2</sub> on nanotextured substrates patterned with nanopillars [Figs. 1(b) and 1(c)]. Conically shaped nanopillars of height  $h$  and interpillar separation (center to center)  $l$  were made of Si(100) and capped with insulator Al<sub>2</sub>O<sub>3</sub> nanospheres 10 nm diameter on

\*Contact author: tamaghna.chowdhury@students.iiserpune.ac.in

†Contact author: artem.mishchenko@gmail.com

‡Contact author: atikur@iiserpune.ac.in

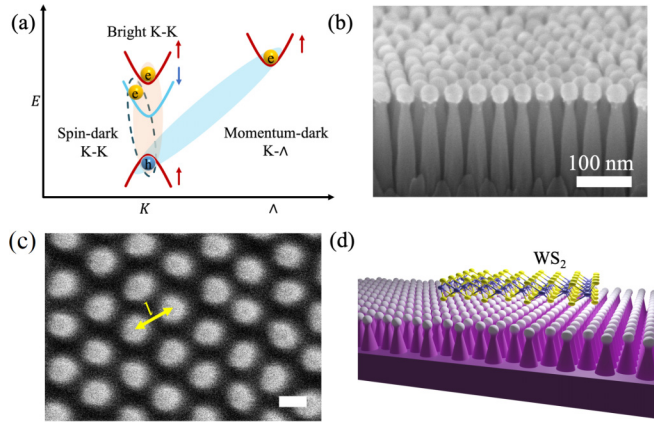


FIG. 1. (a) Schematic showing various excitonic species near the electronic dispersions in the  $K$  and  $\Lambda$  valleys. Arrows indicate the spin orientations. (b) Field emission scanning electron microscope (FESEM) image of the C-99 nanotextured sample (side view). (c) FESEM image of the C-99 substrate as viewed from the top (scale bar is 20 nm). The yellow line shows the interpillar separation  $l$ . (d) Schematic of the substrate with ML  $\text{WS}_2$  placed on top.

top [Figs. 1(b) and 1(c)]. We prepared samples with varied interpillar distances:  $l \approx 25$  nm (sample C-48),  $l \approx 44$  nm (C-99), and  $l \approx 60$  nm (C-132) [20]. By tuning  $l$ , we tune the amount of strain applied to ML  $\text{WS}_2$ . The latter was grown by chemical vapor deposition and was transferred to the top of the nanotextured substrates [21] (see the schematic in Fig. 1(d); see the Supplemental Material, Sec. I [22], for the details of substrate preparation and transfer process).

The PL measurements were performed using a continuous-wave laser with a wavelength of 514.5 nm (2.41 eV) (see Supplemental Material, Sec. II [22]). In the temperature-dependent PL study of ML  $\text{WS}_2$  on the C-99 substrate [Fig. 2(a)], two well-resolved peaks, one at  $\approx 2.01$  eV (FWHM  $\approx 24$  meV) and the other at  $\approx 1.95$  eV (FWHM  $\approx 32$  meV), were observed at 280 K. The peak position and FWHM were extracted from each PL spectrum by fitting with a sum of Gaussian functions (see the Supplemental Material, Sec. III [22]). We attribute the peak at 2.01 eV to a  $KK$  bright exciton ( $X^0$ ) and the peak at 1.95 eV to a negatively charged trion ( $X^-$ ) since ML  $\text{WS}_2$  is an  $n$ -doped semiconductor. We further confirm this assignment by varying the laser excitation power, which alters the exciton density inside the ML  $\text{WS}_2$  channel [23] (see the Supplemental Material, Sec. XIV [22]). As we lower the temperature both  $X^0$  and  $X^-$  blueshift, as reported earlier [24]. At around 200 K, a new peak appears at  $\approx 1.92$  eV. As we further decrease the temperature, the intensity of the new peak increases while that corresponding to  $X^-$  and  $X^0$  diminishes, consistent with the earlier proposal by Feierabend *et al.* for  $K\Lambda$  dark exciton brightening [25]. The 1.92 eV peak can be attributed to (1) a biexciton ( $XX$ ), (2) a defect-bound exciton ( $X^L$ ), or (3) a dark exciton ( $X^D$ ). The exponent  $\alpha$  of the power law dependence (integrated intensity as a function of excitation power) for  $XX$  and  $X^L$  is known to be superlinear ( $\sim 2.0$ ) and sublinear ( $\sim 0.5$ ), respectively [24,26,27]. From the  $I$  vs  $P$  plot, we obtain a value of  $\alpha \sim 1.0$  for the new peak, typical of an exciton [24,26,27] [see Fig. 2(d)]. See Sec. IV of the Supplemental Material [22]

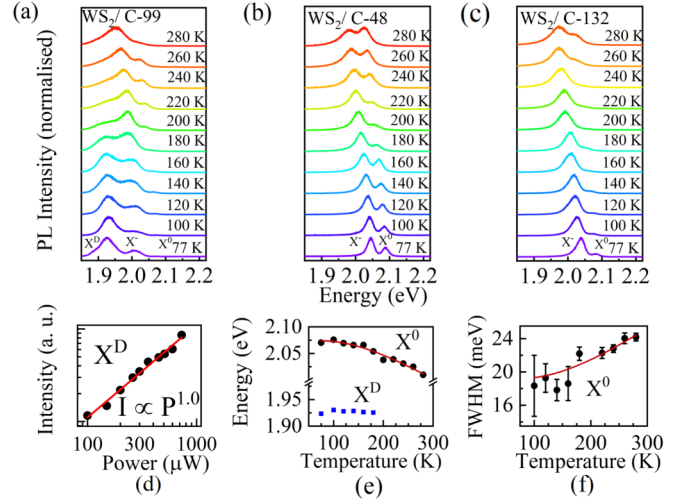


FIG. 2. Temperature-dependent PL spectra of ML  $\text{WS}_2$  placed on top of (a) C-99 (b) C-48, and (c) C-132 substrates. All the spectra are recorded at an excitation power of  $\sim 100$   $\mu\text{W}$ . The spectra are shifted along the  $y$  axis for clarity. (d) The integrated intensity  $I$  of  $X^D$  as a function of excitation power  $P$  fitted with the relation  $I \propto P^\alpha$ , where  $\alpha$  is the exponent. (e) Temperature dependence of the peak position of  $X^0$  (black solid circles) and  $X^D$  (blue solid squares); the temperature dependence of  $X^0$  is fitted with Eq. (1) (red line). (f) FWHM of  $X^0$  as a function of temperature fitted with Eq. (2) (red line).

for the excitation power dependence data for  $X^D$  for another  $\text{WS}_2/\text{C-99}$  sample for which we extracted  $\alpha \sim 1.14$ .

Moreover, the new peak shows no blueshift with increasing excitation power, characteristic of  $X^L$  because of its broad energy distribution [28,29]. However, it showed a redshift due to local heating, a behavior generally seen in excitons [21] (see the Supplemental Material, Sec. V [22]). Furthermore, the new peak also shows anisotropy in circular-polarization-dependent PL, uncharacteristic of  $X^L$  [29,30] (see the Supplemental Material, Sec. VI [22]). Therefore, the new peak is neither  $XX$  nor  $X^L$ . The value of  $\alpha$  and its peak position are similar to those in recent reports of the observation of  $K\Lambda$  dark excitons under compressive strain and strong exciton-phonon coupling [13]. We therefore attribute the peak at  $\sim 1.92$  eV to  $X^D$ . Temperature-dependent PL data of another ML  $\text{WS}_2/\text{C-99}$  sample, for which we have also observed the  $X^D$  peak, is included in Sec. XVI of the Supplemental Material [22]. We performed a similar study for the other two samples, namely, C-48 and C-132 [Figs. 2(b) and 2(c) respectively]. For the C-48 and C-132 samples, we observed  $X^0$  and  $X^-$  peaks at every temperature, but no new peaks were observed as we lowered the temperature to 77 K. The temperature dependence of the peak position of  $X^0$  in the C-99 sample was studied in detail [Fig. 2(e)].

The temperature dependence can be described by the phenomenological model proposed by O'Donnell and Chen [31]:

$$E(T) = E(0) - S \langle \hbar\omega \rangle \left( \coth \frac{\langle \hbar\omega \rangle}{k_B T} - 1 \right), \quad (1)$$

where  $E(T)$  is the resonance energy of  $X^0$  at temperature  $T$ ,  $S$  is the dimensionless exciton-phonon coupling constant,  $k_B$

is the Boltzmann constant, and  $\langle \hbar\omega \rangle$  is the average phonon energy responsible for the coupling. By fitting the experimental data we obtained the parameters  $E(0) = 2.074 \pm 0.003$  eV,  $S = 3.65 \pm 0.98$ , and  $\langle \hbar\omega \rangle = 43 \pm 10$  meV. The value of  $\langle \hbar\omega \rangle$  is close to the energy of the  $E'$  phonon ( $\sim 44$  meV) mode of ML WS<sub>2</sub>. This suggests that the  $E'$  phonon mode is crucial in the exciton-phonon coupling. Note that the peak position of  $X^D$  changes by only  $\sim 2$  meV as we increase the temperature from 77 to 180 K, whereas in the same temperature range, the  $X^0$  peak position changes by  $\sim 20$  meV. This observation aligns with our theoretical calculations (see Fig. S13 in the Sec. X of the Supplemental Material [22]), which shows that the electronic direct band gap at the  $K$  point changes at a much faster rate with temperature in comparison to the indirect  $K - \Lambda$  band gap.

To determine the strength of exciton-phonon coupling, the evolution of the FWHM of  $X^0$  was fitted by a phonon-induced broadening model [Fig. 2(f)] [32,33]:

$$\gamma = \gamma_0 + c_1 T + \frac{c_2}{e^{\frac{\hbar\omega}{k_B T}} - 1}, \quad (2)$$

where  $\gamma_0$  is the intrinsic FWHM, the linear term in  $T$  is due to the interaction of acoustic phonon modes, and the last term describes the interaction with optical phonon modes. The linear term is negligible compared to the last term, as formulated in [34].  $c_2$  is the measure of the exciton-optical phonon coupling strength. The value of  $\hbar\omega$  obtained by fitting Eq. (1) was used for fitting Eq. (2). The value of  $c_2$  obtained by fitting Eq. (2) is  $26.5 \pm 4.6$  meV and is significantly higher than the previously reported value of 6.5 for ML WS<sub>2</sub> [32]. This higher value of  $c_2$  further confirms the strong exciton and  $E'$  phonon mode coupling in the WS<sub>2</sub>/C-99 sample. See Sec. VII in the Supplemental Material [22] for the analysis for the C-48 and C-132 samples.

We further performed a temperature-dependent Raman study for the C-99 sample. The various Raman peaks ( $E'$ , 2LA,  $A_1'$ ) were analyzed with multiple Lorentzian functions [35] (Fig. 3(a); see the Supplemental Material, Sec. VIII [22], for fitting details). The  $E'$  mode showed an unusual blueshift and decreasing linewidth with increasing temperature [see Figs. 3(b) and 3(c)]. This anomalous behavior of the  $E'$  phonon mode is related to electron-phonon coupling [36–38]. The Raman linewidth with temperature is generally explained by the anharmonic cubic equation [39,40]:

$$\gamma_{\text{ph}}(T) = \gamma_0 + C \left[ 1 + 2f_- \left( \frac{\hbar\omega_0}{2k_B T} \right) \right], \quad (3)$$

where  $\gamma_{\text{ph}}(T)$  is the linewidth at temperature  $T$ ,  $\gamma_0$  is the linewidth at  $T = 0$  K,  $\hbar\omega_0$  is the  $E'$  phonon energy,  $f_{\pm}(x) = \frac{1}{e^x \pm 1}$ , and  $C$  is a constant. Equation (3) is simulated in the inset of Fig. 3(c) (green curve). The  $E'$  phonon modes show an opposite trend which is not explained by Eq. (3) because it takes into account only phonon-phonon interaction  $\gamma_{\text{ph}}$  and not the electron-phonon interaction  $\gamma_{e\text{-ph}}$  term [41].  $\gamma_{e\text{-ph}}(T)$  is described by the following equation [37]:

$$\gamma_{e\text{-ph}}(T) = \gamma_{e\text{-ph}}(0) \left[ f_+ \left( \frac{-\hbar\omega_0}{2k_B T} \right) - f_+ \left( \frac{\hbar\omega_0}{2k_B T} \right) \right], \quad (4)$$

where  $\gamma_{e\text{-ph}}(0)$  is the linewidth at  $T = 0$  K due to electron-phonon coupling. In the inset of Fig. 3(c), the red curve is

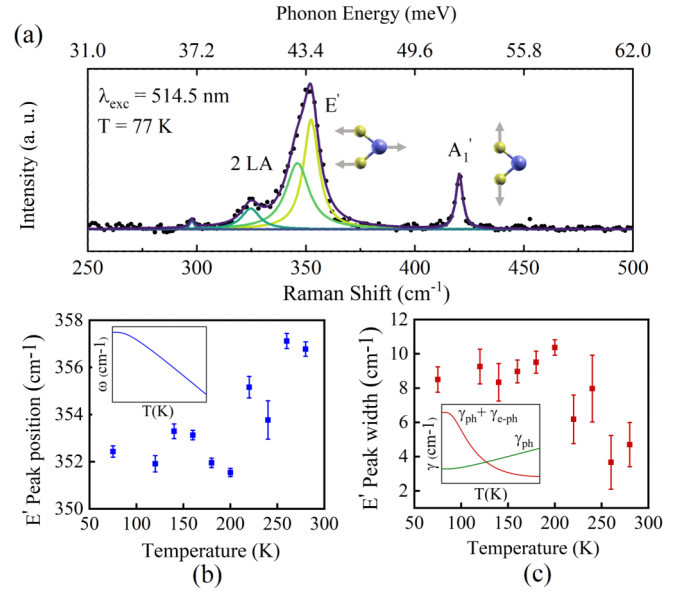


FIG. 3. (a) Raman spectra of ML WS<sub>2</sub> placed on top of a C-99 substrate at 77 K. Various peaks are labeled according to Ref. [35]. The main vibrational modes  $E'$  and  $A_1'$  are shown in the schematic. The blue and yellow balls represent tungsten and sulfur atoms, respectively. Anomalous behavior of the  $E'$  peak (b) position and (c) width as a function of temperature. Simulated  $\omega_{\text{ph}}$  and  $\gamma_{\text{ph}}$  are shown in the insets of (b) (blue curve) and (c) (green curve), respectively.  $\gamma(T) = \gamma_{\text{ph}} + \gamma_{e\text{-ph}}$  (red curve) is simulated in the inset of (c).

simulated with  $\gamma(T) = \gamma_{\text{ph}} + \gamma_{e\text{-ph}}$  and closely resembles the experimental data, thus showing the role of electron-phonon coupling. The phonon-phonon interaction term in the Raman frequency,  $\omega_{\text{ph}}(T) = \omega_0 - D[1 + 2f_- (\frac{\hbar\omega_0}{2k_B T})]$  [41], where  $\omega_0$  is the frequency at  $T = 0$  K and  $D$  is a constant, is simulated in the inset of Fig. 3(b) (blue curve) to show the anomalous behavior of the  $E'$  peak position.

To understand the effect of strain on the electronic band structure of ML WS<sub>2</sub> we computed electronic band structure of WS<sub>2</sub> within the framework of DFT using a fully relativistic norm-conserving pseudopotential with Perdew-Burke-Ernzerhof (PBE) exchange-correlation functionals alongside plane waves, as implemented in the QUANTUM ESPRESSO package [42–51] (Fig. 4(a); see the Supplemental Material, Sec. X [22]). With increasing tensile (compressive) strain, the CBM and CBM + 1 at  $K$  shift down (up), while the CBM at  $\Lambda$  shifts up (down). The  $K$  VBM moves up (down) on application of tensile (compressive) strain [Fig. 4(a)]. We denote the direct band gap at  $K$  between CBM + 1 and VBM as  $E^{KK}$  and the indirect band gap at  $\Lambda$  as  $E^{K\Lambda}$ . Note that, in the electronic band structure of the unstrained WS<sub>2</sub>, the  $\Lambda$  CBM is at higher energy than the CBM + 1 at  $K$  by  $E^{K\Lambda} - E^{KK} = \Delta E^{K\Lambda} \sim 47$  meV. To get into the exciton picture [Fig. 4(b)] from the electron-hole picture (as described in Refs. [8,12]), we need to calculate the binding energy  $E_b$  of the excitons. To this end, we employ the effective mass model [52]:

$$E_b = \frac{\mu e^4}{2\hbar^2 \epsilon^2 (n - \frac{1}{2})^2}, \quad (5)$$

where  $\frac{1}{\mu} = \frac{1}{m_e} + \frac{1}{m_h}$  is the exciton reduced mass and  $m_h$  and  $m_e$  are the effective masses of holes and electrons,

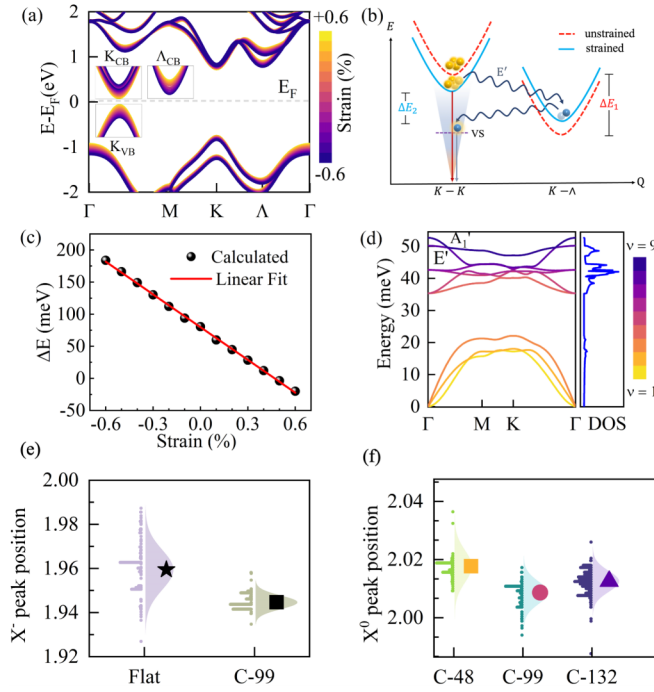


FIG. 4. (a) DFT computed electronic band structure of ML WS<sub>2</sub> with different strain values. (b) Schematic showing the  $E'$  phonon mediated scattering of the bright  $K-K$  excitons to dark  $K-\Lambda$  excitons due to tensile strain. The  $K-\Lambda$  excitons then decay to a virtual state (dotted violet line marked as VS) inside the light cone (shaded area) by emitting phonons and finally recombine radiatively from the VS by emitting photons. (c)  $\Delta E$  as a function of strain on ML WS<sub>2</sub>. (d) Calculated phonon dispersion (left panel) and phonon density of states (DOS; right panel).  $\nu$  represents the phonon band index. (e) Mean peak position of  $X^-$  in ML WS<sub>2</sub> on top of SiO<sub>2</sub>/Si (flat) and C-99 extracted from the PL map. (f) Mean peak position of  $X^0$  in ML WS<sub>2</sub> on top of C-48, C-99, and C-132 extracted from the PL map. The normal distribution and the raw data points are also shown.

respectively.  $\epsilon$  is the dielectric constant of ML WS<sub>2</sub>,  $e$  is the electron charge, and  $n$  is the principal quantum number. Using Eq. (5), we find  $E_b$  of  $X^0$  and  $X^D$  of  $\sim 310$  and  $438$  meV, respectively (see the Supplemental Material, Secs. X and XI [22], for the details of the calculation). Also, we introduce the center-of-mass momentum  $\mathbf{Q} = \mathbf{k}_2 - \mathbf{k}_1$ , where  $\mathbf{k}_1$  and  $\mathbf{k}_2$  are momenta of two bound particles. Now, if we visualize the scenario in the excitonic picture, the bright exciton state is formed at  $K-K$ , at the energy position  $E_{\text{exc}}^{KK} = E^{KK} - E_b^{X^0}$ , and the dark exciton state is formed at  $K-\Lambda$ , at the energy position  $E_{\text{exc}}^{K\Lambda} = E^{K\Lambda} - E_b^{X^D}$  [12]. Our calculations show that, in the unstrained sample, the dark state is below the bright state by an energy of  $E_{\text{exc}}^{KK} - E_{\text{exc}}^{K\Lambda} = \Delta E_1 \sim 81$  meV. Under tensile (compressive) strain, the excitonic states at  $K-K$  and  $K-\Lambda$  go down (up) and up (down), respectively. The change in  $\Delta E$  as a function of strain is plotted in Fig. 4(c) (the values used to generate this plot can be found in the Supplemental Material, Sec. X [22]). The fitting shows an  $\sim 170 \pm 1.4$  meV change in  $\Delta E$  with 1% applied strain. Note that strain has little influence on  $E_b$  [12,53]. As the PBE exchange-correlation functional underestimates the band gap, we also calculate the band structure using a hybrid functional. The behavior of the band

structure with strain remains consistent irrespective of the functional used (see the Supplemental Material, Sec. X [22]).

On optically exciting a coherent exciton population at  $K-K$ , bright excitons are formed. Incoherent excitons are then formed at  $K-\Lambda$  by phonon-assisted scattering of excitons from  $K-K$ , where a phonon compensates for the energy and momentum mismatch [Fig. 4(b)] [14]. However, in the unstrained case, phonon modes with energy  $\Delta E_1 \sim 81$  meV are not available [Fig. 4(d)]; therefore, excitons are not formed at  $K-\Lambda$ . On applying tensile strain (theoretically) on the ML WS<sub>2</sub>, we observe that  $\Delta E$  decreases, and under an  $\sim 0.21\%$  strain the value of  $\Delta E_1$  is reduced to  $\Delta E_2 \sim 44$  meV, thereby making the optical phonons accessible to couple with the exciton for phonon-assisted scattering. To estimate the amount of strain on ML WS<sub>2</sub> on top of the C-99 substrate due to nanopillars, PL mapping was done, and the average peak position of  $X^-$  in the C-99 sample was compared with the average  $X^-$  peak position in ML WS<sub>2</sub> on top of flat SiO<sub>2</sub>/Si [Fig. 4(e)]. Therefore, we can experimentally estimate that ML WS<sub>2</sub> on top of C-99 is under a tensile strain of  $\sim 0.15\%$ , which is in very close agreement with the theoretical value of  $\sim 0.21\%$  (see the Supplemental Material, Sec. XII, for the details of strain determination [22]). In the C-99 sample, phonon-assisted scattering of excitons from  $K-K$  to  $K-\Lambda$  is possible, thereby forming a population of dark excitons. The scattering process is illustrated in the schematic in Fig. 4(b). An  $E'$  phonon with momentum  $K-\Lambda$  and energy  $\sim 44$  meV can make this scattering possible. The calculated phonon density of states shows a large number of phonon states available at  $\sim 44$  meV, thereby making this scattering more favorable (Fig. 4(d); see the Supplemental Material, Sec. X, for the details of the phonon calculation [22]). Note that change in phonon energy with strain is very negligible [54]. To estimate the scattering strength we calculate the electron-phonon matrix element  $g_{mn}^{\nu}(\mathbf{k}, \mathbf{q})$  [Figs. 5(a) and 5(b)] using the formalism described in Refs. [55–57]:

$$g_{mn}^{\nu}(\mathbf{k}, \mathbf{q}) = \langle \psi_{m, \mathbf{k}+\mathbf{q}} | \partial_{\mathbf{q}\nu} V | \psi_{n\mathbf{k}} \rangle, \quad (6)$$

where  $\psi_{n\mathbf{k}}$  is the electronic wave function of the  $n$ th band at the  $\mathbf{k}$  point of the Brillouin zone,  $\nu$  is the phonon band index, and  $\partial_{\mathbf{q}\nu} V$  is the derivative of the self-consistent potential associated with the  $E'$  phonon of momentum  $\mathbf{q}$ . Here, we consider the hole to be fixed at the  $K$  VBM [Fig. 1(a)] and take into account the scattering of electrons from CBM + 1 at  $K$  to the  $\Lambda$  CBM, with a phonon of momentum  $\mathbf{q} = \mathbf{K} - \Lambda$  and the energy value  $\Delta E_2$  being equal to the energy of the  $E'$  phonon mode. Two degenerate  $E'$  phonon modes ( $\nu = 6, 7$ ) with momentum  $K-\Lambda$  show significant coupling strength  $\sim 28$  meV for the scattering under concern [Fig. 5(c)]. We note that this value is comparable to the experimentally estimated exciton-phonon coupling strength reported in the previous paragraphs. The dark excitons at  $K-\Lambda$  then can scatter nonradiatively to a virtual state inside the light cone at  $K-K$  by emitting phonons. Once inside the light cone, the dark excitons can decay radiatively from the virtual state by emitting photons, thus leaving their signature in the PL spectra. The  $X^D$  peak was not observed in ML WS<sub>2</sub>/C-48 and C-132 samples [Figs. 2(b) and 2(c)] because the imparted tensile strain was  $\sim 0.04\%$  and  $0.08\%$ , respectively (calculated by comparing the average  $X^0$  positions in Fig. 4(f); see the Supplemental Material, Sec. XII,

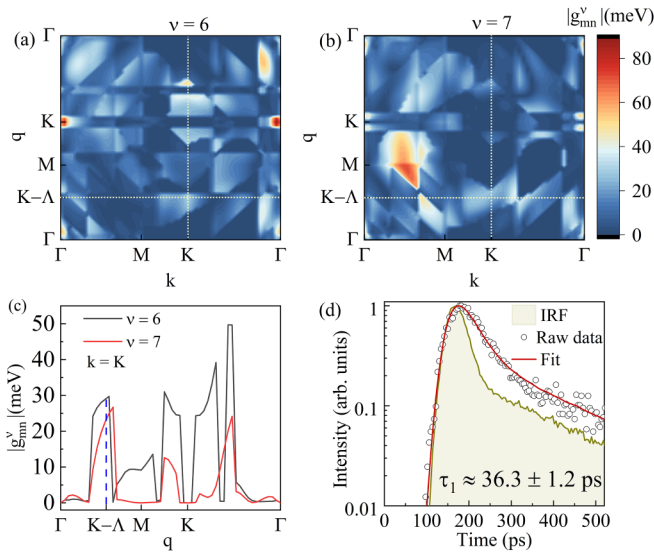


FIG. 5. (a) and (b) Calculated  $g_{mn}^{\nu}$  values for two degenerate  $E'$  phonon modes with  $\nu = 6$  and 7, respectively, which are responsible for the scattering of electrons from CBM+1 at  $K$  to CBM at the  $\Lambda$  valley. (c) Line cut along  $k = K$  from (a) and (b) to show  $g_{mn}^{\nu}$  along the phonon momentum  $q$ , in the  $\Gamma \rightarrow M \rightarrow K \rightarrow \Gamma$  direction. The blue dashed line shows the  $g_{mn}^{\nu}$  of  $q = K - \Lambda$  at  $k = K$ . (d) TRPL measurement on ML WS<sub>2</sub> at 60 K to determine the lifetime of  $X^D$ .

for the details of strain determination [22]). So the  $\Delta E$  value was not close to the energy of any available phonon mode which can open the scattering channel from the  $K - K$  to  $K - \Lambda$  points. To elucidate the kinetics of  $X^D$ , we performed time-resolved PL (TRPL) on the ML WS<sub>2</sub> on top of the C-99 substrate [Fig. 5(d)]. The lifetime  $\tau$  of  $X^D$  is estimated to be  $\tau \approx 36.3 \pm 1.2$  ps (see the Supplemental Material, Sec. XIII, for the measurement and fitting details [22]), which is 30 times larger than the reported decay time of a neutral exciton  $X^0$  ( $\tau \sim 1$  ps at  $T = 60$  K) [58,59] as  $X^D$  is the excitonic ground state of ML WS<sub>2</sub> [11,13].

In summary, we reported the experimental observation of momentum-forbidden  $K\Lambda$  dark excitons by applying tensile strain on ML WS<sub>2</sub> using a nanotextured substrate. Our model shows that the  $K\Lambda$  dark excitons in both WS<sub>2</sub> and WSe<sub>2</sub> can be brightened by the application of tensile strain, thereby

establishing the universality across W-based TMDs. Also, TMDs are prone to buckling under compressive strain [60], and compressive strain is difficult to create at lower temperatures, which is necessary for the brightening of  $K\Lambda$  dark excitons [13]. Rather, TMDs can endure high tensile strain and are easy to create [61]. Therefore, our work paves the way for more application-oriented modulation of the  $K\Lambda$  dark exciton, which, being the excitonic ground state, strongly affects exciton dynamics in W-based materials.

A.M. acknowledges the support of the European Research Council (ERC) under the European Union's Horizon 2020 research and innovation program (Grant Agreement No. 865590). This research used electron microscopy facilities of the Center for Functional Nanomaterials (CFN), which is a U.S. Department of Energy Office of Science User Facility at Brookhaven National Laboratory under Contract No. DE-SC0012704. A.R. acknowledges funding support from DST SERB Grant no. CRG/2021/005659 and partial funding support under Indo-French Centre for the Promotion of Advanced Research (CEFIPRA) Project No. 6104-2. We thank the National Supercomputing Mission (NSM) for providing computing resources for “PARAM Bramha” at IISER Pune, which is implemented by C-DAC and supported by the Ministry of Electronics and Information Technology (MeitY) and Department of Science and Technology (DST), Government of India. The authors would like to acknowledge funding from the National Mission on Interdisciplinary Cyber-Physical Systems (NM-ICPS) of the DST, Government of India, through the I-HUB Quantum Technology Foundation, Pune, India. We thank Professor Sandip Ghosh, DCMPS, TIFR Mumbai, India, for his help with polarization PL experiments and valuable discussions. T.C. and S.C. thank PMRF, Ministry of Education, Government of India, for the research fellowship (ID's No. 0700441 and No. 0701511). T.C. is grateful for the research reported here, funded by the Commonwealth Scholarship Commission and the Foreign, Commonwealth, and Development Office in the UK (Split-site fellowship grant no. INCN-2021-049). All views expressed here are those of the author(s), not the funding body. P.G. acknowledges support from the Abdus Salam ICTP through the Associates Programme and from the Simons Foundation through Grant No. 284558FY19.

[1] K. F. Mak and J. Shan, Photonics and optoelectronics of 2D semiconductor transition metal dichalcogenides, *Nat. Photon.* **10**, 216 (2016).  
 [2] K. F. Mak, C. Lee, J. Hone, J. Shan, and T. F. Heinz, Atomically thin MoS<sub>2</sub>: A new direct-gap semiconductor, *Phys. Rev. Lett.* **105**, 136805 (2010).  
 [3] J. S. Ross, S. Wu, H. Yu, N. J. Ghimire, A. M. Jones, G. Aivazian, J. Yan, D. G. Mandrus, D. Xiao, W. Yao, and X. Xu, Electrical control of neutral and charged excitons in a monolayer semiconductor, *Nat. Commun.* **4**, 1474 (2013).  
 [4] A. Splendiani, L. Sun, Y. Zhang, T. Li, J. Kim, C.-Y. Chim, G. Galli, and F. Wang, Emerging photoluminescence in monolayer MoS<sub>2</sub>, *Nano Lett.* **10**, 1271 (2010).

[5] K. He, N. Kumar, L. Zhao, Z. Wang, K. F. Mak, H. Zhao, and J. Shan, Tightly bound excitons in monolayer WSe<sub>2</sub>, *Phys. Rev. Lett.* **113**, 026803 (2014).  
 [6] A. Ramasubramaniam, Large excitonic effects in monolayers of molybdenum and tungsten dichalcogenides, *Phys. Rev. B* **86**, 115409 (2012).  
 [7] H.-P. Komsa and A. V. Krasheninnikov, Effects of confinement and environment on the electronic structure and exciton binding energy of MoS<sub>2</sub> from first principles, *Phys. Rev. B* **86**, 241201(R) (2012).  
 [8] E. Malic, M. Selig, M. Feierabend, S. Brem, D. Christiansen, F. Wendler, A. Knorr, and G. Berghäuser, Dark excitons in transition metal dichalcogenides, *Phys. Rev. Mater.* **2**, 014002 (2018).

- [9] M. Selig, G. Berghäuser, A. Raja, P. Nagler, C. Schüller, T. F. Heinz, T. Korn, A. Chernikov, E. Malic, and A. Knorr, Excitonic linewidth and coherence lifetime in monolayer transition metal dichalcogenides, *Nat. Commun.* **7**, 13279 (2016).
- [10] S. Brem, A. Ekman, D. Christiansen, F. Katsch, M. Selig, C. Robert, X. Marie, B. Urbaszek, A. Knorr, and E. Malic, Phonon-assisted photoluminescence from indirect excitons in monolayers of transition-metal dichalcogenides, *Nano Lett.* **20**, 2849 (2020).
- [11] J. Madéo, M. K. L. Man, C. Sahoo, M. Campbell, V. Pareek, E. L. Wong, A. Al-Mahboob, N. S. Chan, A. Karmakar, B. M. K. Mariserla, X. Li, T. F. Heinz, T. Cao, and K. M. Dani, Directly visualizing the momentum-forbidden dark excitons and their dynamics in atomically thin semiconductors, *Science* **370**, 1199 (2020).
- [12] M. Feierabend, Z. Khatibi, G. Berghäuser, and E. Malic, Dark exciton based strain sensing in tungsten-based transition metal dichalcogenides, *Phys. Rev. B* **99**, 195454 (2019).
- [13] S. B. Chand, J. M. Woods, E. Mejia, T. Taniguchi, K. Watanabe, and G. Grosso, Visualization of dark excitons in semiconductor monolayers for high-sensitivity strain sensing, *Nano Lett.* **22**, 3087 (2022).
- [14] M. Selig, G. Berghäuser, M. Richter, R. Bratschitsch, A. Knorr, and E. Malic, Dark and bright exciton formation, thermalization, and photoluminescence in monolayer transition metal dichalcogenides, *2D Mater.* **5**, 035017 (2018).
- [15] K. Zollner, P. E. Faria Junior, and J. Fabian, Strain-tunable orbital, spin-orbit, and optical properties of monolayer transition-metal dichalcogenides, *Phys. Rev. B* **100**, 195126 (2019).
- [16] I. Niehues, R. Schmidt, M. Drüppel, P. Marauhn, D. Christiansen, M. Selig, G. Berghäuser, D. Wigger, R. Schneider, L. Braasch, R. Koch, A. Castellanos-Gomez, T. Kuhn, A. Knorr, E. Malic, M. Rohlfing, S. Michaelis de Vasconcellos, and R. Bratschitsch, Strain control of exciton-phonon coupling in atomically thin semiconductors, *Nano Lett.* **18**, 1751 (2018).
- [17] R. Rosati, R. Schmidt, S. Brem, R. Perea-Causín, I. Niehues, J. Kern, J. A. Preuß, R. Schneider, S. Michaelis de Vasconcellos, R. Bratschitsch, and E. Malic, Dark exciton anti-funneling in atomically thin semiconductors, *Nat. Commun.* **12**, 7221 (2021).
- [18] R. J. Gelly, D. Renaud, X. Liao, B. Pingault, S. Bogdanovic, G. Scuri, K. Watanabe, T. Taniguchi, B. Urbaszek, H. Park, and M. Lončar, Probing dark exciton navigation through a local strain landscape in a WSe<sub>2</sub> monolayer, *Nat. Commun.* **13**, 232 (2022).
- [19] S. Chand, Exciton dynamics, interaction, and transport in monolayers of transition metal dichalcogenides, Ph.D. thesis, City University of New York, 2024.
- [20] A. Rahman, A. Ashraf, H. Xin, X. Tong, P. Sutter, M. D. Eisaman, and C. T. Black, Sub-50-nm self-assembled nanotextures for enhanced broadband antireflection in silicon solar cells, *Nat. Commun.* **6**, 5963 (2015).
- [21] T. Chowdhury, D. Paul, D. Nechiyil, G. M. A. K. Watanabe, T. Taniguchi, G. V. P. Kumar, and A. Rahman, Modulation of trion and exciton formation in monolayer WS<sub>2</sub> by dielectric and substrate engineering, *2D Mater.* **8**, 045032 (2021).
- [22] See Supplemental Material at <http://link.aps.org/supplemental/10.1103/PhysRevB.110.L081405> for additional details on sample preparation, sample characterization, measurement details, fitting methodology and computational methodology. It also includes Refs. [62–77].
- [23] C. Poellmann, P. Steinleitner, U. Leierseder, P. Nagler, G. Plechinger, M. Porer, R. Bratschitsch, C. Schüller, T. Korn, and R. Huber, Resonant internal quantum transitions and femtosecond radiative decay of excitons in monolayer WSe<sub>2</sub>, *Nat. Mater.* **14**, 889 (2015).
- [24] G. Plechinger, P. Nagler, J. Kraus, N. Paradiso, C. Strunk, C. Schüller, and T. Korn, Identification of excitons, trions and biexcitons in single-layer WS<sub>2</sub>, *Phys. Status Solidi RRL* **9**, 457 (2015).
- [25] M. Feierabend, G. Berghäuser, A. Knorr, and E. Malic, Proposal for dark exciton based chemical sensors, *Nat. Commun.* **8**, 14776 (2017).
- [26] J. Shang, X. Shen, C. Cong, N. Peimyoo, B. Cao, M. Eginligil, and T. Yu, Observation of excitonic fine structure in a 2D transition-metal dichalcogenide semiconductor, *ACS Nano* **9**, 647 (2015).
- [27] I. Paradisanos, S. Germanis, N. Pelekanos, C. Fotakis, E. Kymakis, G. Kioseoglou, and E. Stratakis, Room temperature observation of biexcitons in exfoliated WS<sub>2</sub> monolayers, *Appl. Phys. Lett.* **110**, 193102 (2017).
- [28] R. Kaupmees, M. Grossberg, M. Ney, A. Asaithambi, A. Lorke, and J. Krustok, Tailoring of bound exciton photoluminescence emission in WS<sub>2</sub> monolayers, *Phys. Status Solidi RRL* **14**, 1900355 (2020).
- [29] N. Saigal and S. Ghosh, Phonon induced luminescence decay in monolayer MoS<sub>2</sub> on SiO<sub>2</sub>/Si substrates, *Appl. Phys. Lett.* **107**, 242103 (2015).
- [30] N. Saigal and S. Ghosh, Evidence for two distinct defect related luminescence features in monolayer MoS<sub>2</sub>, *Appl. Phys. Lett.* **109**, 122105 (2016).
- [31] K. P. O'Donnell and X. Chen, Temperature dependence of semiconductor band gaps, *Appl. Phys. Lett.* **58**, 2924 (1991).
- [32] F. Cadiz, E. Courtade, C. Robert, G. Wang, Y. Shen, H. Cai, T. Taniguchi, K. Watanabe, H. Carrere, D. Lagarde, M. Manca, T. Amand, P. Renucci, S. Tongay, X. Marie, and B. Urbaszek, Excitonic linewidth approaching the homogeneous limit in MoS<sub>2</sub>-based van der Waals heterostructures, *Phys. Rev. X* **7**, 021026 (2017).
- [33] S. Rudin, T. L. Reinecke, and B. Segall, Temperature-dependent exciton linewidths in semiconductors, *Phys. Rev. B* **42**, 11218 (1990).
- [34] A. Arora, M. Koperski, K. Nogajewski, J. Marcus, C. Faugeras, and M. Potemski, Excitonic resonances in thin films of WSe<sub>2</sub>: From monolayer to bulk material, *Nanoscale* **7**, 10421 (2015).
- [35] A. Berkdemir, H. R. Gutiérrez, A. R. Botello-Méndez, N. Perea-López, A. L. Elías, C.-I. Chia, B. Wang, V. H. Crespi, F. López-Urías, J.-C. Charlier, H. Terrones, and M. Terrones, Identification of individual and few layers of WS<sub>2</sub> using Raman spectroscopy, *Sci. Rep.* **3**, 1755 (2013).
- [36] A. C. Ferrari, Raman spectroscopy of graphene and graphite: Disorder, electron-phonon coupling, doping and nonadiabatic effects, *Solid State Commun.* **143**, 47 (2007).
- [37] N. Bonini, M. Lazzeri, N. Marzari, and F. Mauri, Phonon anharmonicities in graphite and graphene, *Phys. Rev. Lett.* **99**, 176802 (2007).
- [38] D.-H. Chae, B. Krauss, K. Von Klitzing, and J. H. Smet, Hot phonons in an electrically biased graphene constriction, *Nano Lett.* **10**, 466 (2010).

- [39] M. Balkanski, R. F. Wallis, and E. Haro, Anharmonic effects in light scattering due to optical phonons in silicon, *Phys. Rev. B* **28**, 1928 (1983).
- [40] J. Joshi, I. R. Stone, R. Beams, S. Krylyuk, I. Kalish, A. V. Davydov, and P. M. Vora, Phonon anharmonicity in bulk T<sub>d</sub> – MoTe<sub>2</sub>, *Appl. Phys. Lett.* **109**, 031903 (2016).
- [41] S. Paul, S. Karak, M. Mandal, A. Ram, S. Marik, R. P. Singh, and S. Saha, Tailoring the phase transition and electron-phonon coupling in 1T'-MoTe<sub>2</sub> by charge doping: A Raman study, *Phys. Rev. B* **102**, 054103 (2020).
- [42] P. Giannozzi *et al.*, QUANTUM ESPRESSO: A modular and open-source software project for quantum simulations of materials, *J. Phys.: Condens. Matter* **21**, 395502 (2009).
- [43] P. Giannozzi *et al.*, Advanced capabilities for materials modelling with Quantum Espresso, *J. Phys.: Condens. Matter* **29**, 465901 (2017).
- [44] D. R. Hamann, M. Schlüter, and C. Chiang, Norm-conserving pseudopotentials, *Phys. Rev. Lett.* **43**, 1494 (1979).
- [45] Z. Y. Zhu, Y. C. Cheng, and U. Schwingenschlögl, Giant spin-orbit-induced spin splitting in two-dimensional transition-metal dichalcogenide semiconductors, *Phys. Rev. B* **84**, 153402 (2011).
- [46] A. H. MacDonald and S. H. Vosko, A relativistic density functional formalism, *J. Phys. C* **12**, 2977 (1979).
- [47] A. K. Rajagopal and J. Callaway, Inhomogeneous electron gas, *Phys. Rev. B* **7**, 1912 (1973).
- [48] A. D. Corso and A. M. Conte, Spin-orbit coupling with ultrasoft pseudopotentials: Application to Au and Pt, *Phys. Rev. B* **71**, 115106 (2005).
- [49] J. P. Perdew, K. Burke, and M. Ernzerhof, Generalized gradient approximation made simple, *Phys. Rev. Lett.* **77**, 3865 (1996).
- [50] A. Molina-Sánchez and L. Wirtz, Phonons in single-layer and few-layer Mo<sub>2</sub> and WS<sub>2</sub>, *Phys. Rev. B* **84**, 155413 (2011).
- [51] S. Baroni, S. de Gironcoli, A. D. Corso, and P. Giannozzi, Phonons and related crystal properties from density-functional perturbation theory, *Rev. Mod. Phys.* **73**, 515 (2001).
- [52] A. Chernikov, T. C. Berkelbach, H. M. Hill, A. Rigosi, Y. Li, B. Aslan, D. R. Reichman, M. S. Hybertsen, and T. F. Heinz, Exciton binding energy and nonhydrogenic Rydberg series in monolayer WS<sub>2</sub>, *Phys. Rev. Lett.* **113**, 076802 (2014).
- [53] M. Feierabend, A. Morlet, G. Berghäuser, and E. Malic, Impact of strain on the optical fingerprint of monolayer transition-metal dichalcogenides, *Phys. Rev. B* **96**, 045425 (2017).
- [54] Z. Khatibi, M. Feierabend, M. Selig, S. Brem, C. Linderälvy, P. Erhart, and E. Malic, Impact of strain on the excitonic linewidth in transition metal dichalcogenides, *2D Mater.* **6**, 015015 (2018).
- [55] E. R. Margine and F. Giustino, Anisotropic Migdal-Eliashberg theory using Wannier functions, *Phys. Rev. B* **87**, 024505 (2013).
- [56] F. Giustino, M. L. Cohen, and S. G. Louie, Electron-phonon interaction using Wannier functions, *Phys. Rev. B* **76**, 165108 (2007).
- [57] H. Lee, S. Poncé, K. Bushick, S. Hajinazar, J. Lafuente-Bartolome, J. Leveillee, C. Lian, J.-M. Lihm, F. Macheda, H. Mori, H. Paudyal, W. H. Sio, S. Tiwari, M. Zacharias, X. Zhang, N. Bonini, E. Kioupakis, E. R. Margine, and F. Giustino, Electron-phonon physics from first principles using the EPW code, *npj Comput. Mater.* **9**, 156 (2023).
- [58] P. Nagler, M. V. Ballottin, A. A. Mitioglu, M. V. Durnev, T. Taniguchi, K. Watanabe, A. Chernikov, C. Schüller, M. M. Glazov, P. C. M. Christianen, and T. Korn, Zeeman splitting and inverted polarization of biexciton emission in monolayer WS<sub>2</sub>, *Phys. Rev. Lett.* **121**, 057402 (2018).
- [59] C. Robert, D. Lagarde, F. Cadiz, G. Wang, B. Lassagne, T. Amand, A. Balocchi, P. Renucci, S. Tongay, B. Urbaszek, and X. Marie, Exciton radiative lifetime in transition metal dichalcogenide monolayers, *Phys. Rev. B* **93**, 205423 (2016).
- [60] K.-A. N. Duerloo, Y. Li, and E. J. Reed, Structural phase transitions in two-dimensional Mo- and W-dichalcogenide monolayers, *Nat. Commun.* **5**, 4214 (2014).
- [61] A. Castellanos-Gomez, M. Poot, G. A. Steele, H. S. Van Der Zant, N. Agrait, and G. Rubio-Bollinger, Elastic properties of freely suspended MoS<sub>2</sub> nanosheets, *Adv. Mater.* **24**, 772 (2012).
- [62] A. Gurarlan, Y. Yu, L. Su, Y. Yu, F. Suarez, S. Yao, Y. Zhu, M. Ozturk, Y. Zhang, and L. Cao, Surface-energy-assisted perfect transfer of centimeter-scale monolayer and few-layer MoS<sub>2</sub> films onto arbitrary substrates, *ACS Nano* **8**, 11522 (2014).
- [63] N. Lundt, E. Cherotchenko, O. Iff, X. Fan, Y. Shen, P. Bigenwald, A. V. Kavokin, S. Höfling, and C. Schneider, The interplay between excitons and trions in a monolayer of MoSe<sub>2</sub>, *Appl. Phys. Lett.* **112**, 031107 (2018).
- [64] M. Sledzinska, P. Xiao, E. Puig Vilardell, E. C. Angel, M. J. Esplandiú, and C. M. S. Torres, Exciton tuning and strain imaging in WS<sub>2</sub> supported on PDMS micropillars, *Appl. Phys. Lett.* **121**, 253101 (2022).
- [65] K. Wei, Y. Liu, H. Yang, X. Cheng, and T. Jiang, Large range modification of exciton species in monolayer WS<sub>2</sub>, *Appl. Opt.* **55**, 6251 (2016).
- [66] S. Poncé, E. R. Margine, C. Verdi, and F. Giustino, EPW: Electron-phonon coupling, transport and superconducting properties using maximally localized Wannier functions, *Comput. Phys. Commun.* **209**, 116 (2016).
- [67] M. van Setten, M. Giantomassi, E. Bousquet, M. Verstraete, D. Hamann, X. Gonze, and G.-M. Rignanes, The PSEUDODOJO: Training and grading a 85 element optimized norm-conserving pseudopotential table, *Comput. Phys. Commun.* **226**, 39 (2018).
- [68] A. Arora, Magneto-optics of layered two-dimensional semiconductors and heterostructures: Progress and prospects, *J. Appl. Phys.* **129**, 120902 (2021).
- [69] J.-W. Song, K. Yamashita, and K. Hirao, Communication: A new hybrid exchange correlation functional for band-gap calculations using a short-range Gaussian attenuation (Gaussian-Perdue-Burke-Ernzerhof), *J. Chem. Phys.* **135**, 071103 (2011).
- [70] A. Michail, D. Anastopoulos, N. Delikoukos, S. Grammatikopoulos, S. A. Tsirkas, N. N. Lathiotakis, O. Frank, K. Filintoglou, J. Parthenios, and K. Papagelis, Tuning the photoluminescence and Raman response of single-layer WS<sub>2</sub> crystals using biaxial strain, *J. Phys. Chem. C* **127**, 3506 (2023).
- [71] H. R. Gutiérrez, N. Perea-López, A. L. Elías, A. Berkdemir, B. Wang, R. Lv, F. López-Urías, V. H. Crespi, H. Terrones, and M. Terrones, Extraordinary room-temperature photoluminescence in triangular WS<sub>2</sub> monolayers, *Nano Lett.* **13**, 3447 (2013).
- [72] A. A. Mitioglu, P. Plochocka, J. N. Jadcak, W. Escoffier, G. L. J. A. Rikken, L. Kulyuk, and D. K. Maude,

- Optical manipulation of the exciton charge state in single-layer tungsten disulfide, *Phys. Rev. B* **88**, 245403 (2013).
- [73] G. Wang, C. Robert, M. M. Glazov, F. Cadiz, E. Courtade, T. Amand, D. Lagarde, T. Taniguchi, K. Watanabe, B. Urbaszek, and X. Marie, In-plane propagation of light in transition metal dichalcogenide monolayers: Optical selection rules, *Phys. Rev. Lett.* **119**, 047401 (2017).
- [74] E. Liu, J. van Baren, T. Taniguchi, K. Watanabe, Y.-C. Chang, and C. H. Lui, Valley-selective chiral phonon replicas of dark excitons and trions in monolayer WSe<sub>2</sub>, *Phys. Rev. Res.* **1**, 032007(R) (2019).
- [75] R. Kesarwani, K. B. Simbulan, T.-D. Huang, Y.-F. Chiang, N.-C. Yeh, Y.-W. Lan, and T.-H. Lu, Control of trion-to-exciton conversion in monolayer WS<sub>2</sub> by orbital angular momentum of light, *Sci. Adv.* **8**, eabm0100 (2022).
- [76] K. M. McCreary, A. T. Hanbicki, S. Singh, R. K. Kawakami, G. G. Jernigan, M. Ishigami, A. Ng, T. H. Brintlinger, R. M. Stroud, and B. T. Jonker, The effect of preparation conditions on Raman and photoluminescence of monolayer WS<sub>2</sub>, *Sci. Rep.* **6**, 35154 (2016).
- [77] S. Chatterjee, S. Das, G. Gupta, K. Watanabe, T. Taniguchi, and K. Majumdar, Probing biexciton in monolayer WS<sub>2</sub> through controlled many-body interaction, *2D Mater.* **9**, 015023 (2022).